Crystallization and Melting Processes in Vulcanized Stretched Natural Rubber

3 AUTHORS, INCLUDING:

J. Rault
Université Paris-Sud 11

76 PUBLICATIONS   **1,237** CITATIONS

Crystallization and Melting Processes in Vulcanized Stretched Natural Rubber

S. Trabelsi, P.-A. Albouy, and J. Rault*

*Laboratoire de Physique des Solides, UMR 8502, Université de Paris-Sud,
Bât. 510, 91405 Orsay, France*

ABSTRACT: We have studied, by simultaneous force and WAXS measurements, crystallization and melting properties of stretched natural poly *cis*-isoprene, vulcanized at different rates, in static and dynamic deformations. The overall effects of increasing N_C, the number of monomers between cross-link bridges, is to slow the kinetics of crystallization and to decrease the melting temperature, crystallites sizes, crystallinity, and mechanical hysteresis. The origin of these properties is discussed. The morphologies of vulcanized rubbers during static and dynamic deformations are very similar. The process of crystallization (and melting) occurs during these two types of deformation by nucleation (and disappearance) of crystallites with constant sizes. The role of the affine deformation of the cross-link network on the crystallites dimension is pointed out. During cyclic deformations, real time measurements during stretching and recovery permit one to conclude that mechanical hysteresis is due only to the chains crystallization or more exactly to the supercooling (difference between melting and crystallization temperatures). During stress hardening, the form of the stress−strain curve $\sigma \sim \lambda^2$ is explained following the Flory idea. Each new crystallite formed during stretching is considered as a cross-link. The Flory stress-induced crystallization model is discussed. In the Appendix, we describe the new effect called "inverse yielding" observed in weakly cross-linked rubbers.

1. Introduction

Stress-induced crystallization (SIC) of polymers have been studied for more than half a century, by different techniques: X-ray scattering,[1−4] infrared spectroscopy,[5,6] birefringence,[6−10] electron microscopy,[11−17] dilatometry,[18−22] and stress relaxation.[18,23−25] In crystallizable elastomers, it is recognized that this phenomenon explains the interesting properties of these materials such as tearing resistance and high stress at break.[26−29] Despite the great amount of work done on stretched polymers, in particular on dry vulcanized rubbers, the morphology of the semicrystalline phase appearing during melting and crystallization processes by changing temperature or deformation, has not been studied in details. By small-angle X-ray scattering[3] (SAXS) and transmission electron micoscopy[11−15] (TEM), authors have described the supracrystalline organization of the semicrystalline structure (spherulitic, fibrillar) but the evolution of crystallinity and crystallites dimensions as a function of temperature, draw ratio, and cross-linking density has not been studied in details.

Over the past 6 decades, numerous theoretical studies have been devoted to the low and high elongation behavior of rubberlike networks. Most of the constitutive models,[30−33] proposed to capture the large elongation behavior, do not take into account the SIC phenomenon which could appear in isotatic polymers above the glass temperature. Only a few authors following the Flory pioneer work gave thermodynamic models of the stress-induced crystallization in polymers networks at equilibrium.[34−40] These theories predict rather well the increase of melting temperature T_m with the draw ratio and the stress relaxation during crystallization; however, they fail in quantitative regards. These SIC theories assume that the system is at equilibrium (fixed extension), they are not supposed to apply to materials during stretching and cyclic deformation at constant strain rate for example. To our knowledge, there is no common theory, which covers both thermally, and strain-induced crystallization in polymer networks, and which predicts the semicrystalline morphology and the mechanical properties.

In comparison, the semicrystalline state of isotropic polymers is well documented.[41−43] In these materials the dependences of the crystalline l_C, and amorphous size domains l_a, with the supercooling, annealing temperature, and molecular weight distribution are very well-known.[44−46]

In vulcanized rubber, the chains are cross-linked and no individual chain can be defined; one wonders what is the physical process which limits the crystallinity and what is the influence of the cross-linking density and deformation on parameters (l_C,χ) of the semicrystalline state in stretched networks, compared to isotropic polymers.

During mechanical cycles, Toki et al. have been the pioneers in investigating the variation of crystallinity index and chain orientation during slow cycle of stretching using wide-angle X-rays scattering[47−49] technique. In their study, the morphology of the crystalline structure at a nanoscale has not been measured and compared to that observed in static deformation.

The aim of this paper is to describe the semicrystalline state of a crystallizable elastomer in different experimental conditions: at fixed draw ratio and during slow dynamic deformation. Natural rubber (poly(*cis*-isoprene)) with three different cross-linking densities has been studied by simultaneous mechanical and (WAXS) measurements.

The paper is divided as follow. In section 2, the rubber materials and the techniques are described. In section

Table 1

| ingredient | natural rubber with different density | | |
	sample **I**	sample **II**	sample **III**
g of natural rubber (TSR 20)	100	100	100
g of stearic acid	2	2	2
g of zinc oxide	5	5	5
g of antioxidant (6PPD)	1	1	1
g of sulfur	0.8	1.2	2
g of accelerator (CBS)	0.8	1.2	2
Young modulus E (MPa)	1.084	1.41	2.4
swelling $\nu_s * 10^2$ mol/m^3	0.40	0.57	0.94
Young modulus " "	0.41	0.62	0.97
no. of monomers between two cross-linked $N_C = (\rho/M_0 \nu_s)$ monomers	$N_C = 335$	$N_C = 238$	$N_C = 145$

3, the morphology of the semicrystalline state (crystallites sizes, crystallite orientation, crystallinity) is determined during crystallization and melting at constant length. The influence of cross-links density and deformation on crystallinity and crystallite sizes is described. Section 4 is devoted to cyclic deformation at low strain rate. Crystallite sizes and orientation are compared to those obtained at equilibrium. The new effect of inverse yield appearing in weakly vulcanized rubber is described. The correlation between relaxation stress and crystallinity is given and the origin of the critical draw ratios at which the beginning of crystallization and the end of melting occur is discussed. Finally, in section 5, one explains the effect of cross-linking degree on the mechanical hysteresis of natural rubber.

2. Experimental Section

2.1. Material. The materials (supplied by Michelin Co.) have been obtained by sulfur vulcanization of natural rubber. The formulations are given in Table 1, all samples called here after **I**, **II**, and **III** have the same concentration of ingredients (stearic acid, zinc oxide, antioxidant) and only the concentrations of sulfur and accelerator (CBS) are different. The cross-link density, ν_s, has been determined by swelling in toluene and by Young modulus measurements. These two methods give very similar results. N_C the number of monomers between cross-links is deduced from ν_s where $N_C = (\rho/M_0 \nu_s)$; $M_0 = 68$ is the molecular weight of the monomer, and $\rho = 0.92$ g/cm^3 is the density. The samples (length 30 mm) have the typical dumbbell form, the thickness, $t = 1.5$ mm, is close to the optimum thickness for diffraction measurements using Cu Kα radiation.[50] The effective draw ratio λ is determined by measuring the distance between ink marks on the samples during deformation.

2.2. Instruments and Procedures. (a) Static Measurements. A homemade oven with X-rays transparent Kapton windows, vacuum insulation, and external force measurement is used for isothermal crystallization. This oven is connected to two thermostated baths which permit quenching the sample from +100 to −30 °C in short times (typically 40 °C/min). The sample in this experimental set up can be extended up to the draw ratio $\lambda = 8$. This oven is mounted on an X-ray generator equipped with homemade parallel optics and a conventional $\theta-2\theta$ goniometer (conventional generator, xenon-filled proportional counter) or in front of a parallel beam optics (rotating anode generator, detection by photostimulated image plates) or by an indirect illumination CCD camera (Princeton Instrument). This experimental setup enables us to measure simultaneously tensile stress and WAXS spectra.

(b) Dynamic Measurements. A homemade stretching machine with symmetric extension is used at room temperature for deformation at strain rate from d$\lambda/$d$t = 0.033$ min^{-1} ($\dot{\epsilon} = 1$ mm/min) to 20 min^{-1}. High resolution is necessary for real-time measurements of reflection profiles during cyclic deformation; for this purpose this drawing machine was

mounted at the station D 43 of the synchrotron LURE, coupled with the above-mentioned CCD camera (see Figure 1 for a general view of the experimental setup). The drawing machine is titled to obtain the (002) reflection as shown in the figure. For the measurements of the Bragg-scattered intensities (i.e., crystallinity), the setup is mounted on a rotating anode generator, and the detection is performed with a homemade linear counter. During stretching, the thickness and then the absorption of the sample decrease. The measurements of the absorption taken by the photodiode, located along the beam axis behind the sample, are used to normalize the scattered intensities.

(c) Data Corrections and Analysis. Absorption Measurements. It is known that diffracted intensity depends on the sample thickness t, material absorption coefficient μ and primary beam intensity I_0 by a factor $I_0 t \exp(-\mu t)$ if one neglects any angular dependence.[51] During the cycle of deformation, it is necessary to correct the continuous variations of the sample thickness t and the incident beam fluctuations. The signal provided by the photodiode placed behind the sample is proportional to $I_0 \exp(-\mu t)$. By measuring the primary beam intensity I_0 at regular time intervals, it is thus possible to evaluate simultaneously t and the corresponding absorption correction, knowing the initial sample thickness; variations in μ due to the changes of mass density during crystallization are presently negligible.

Reflection Profiles. The crystal structure is orthorhombic[52] (space group *Pbca*). The (002) diffraction line originates from the beam reflection on lattice planes perpendicular to the c chain axis, this meridian reflection is observed when the sample is tilted as shown in Figure 1. Its width is related to the average crystallite dimension l_{002}, (often called in the literature the stem length l_C, used to describe the crystallite size when the chains are folded or extended in the crystallite). The azimuthal profile is directly linked to the crystallite orientation function. The intense (200) and (120) reflections correspond to lattice planes parallel to the chain direction. It is well-known that reflections of low indices and high intensity are associated with denser planes and generally correspond to naturally occurring crystallographic surfaces. For this reason, in the following, the crystallites growth faces are supposed to be parallel to the (100), (120), and (001) planes.

The amorphous background is removed using the noncrystallized sample signal as reference; the instrumental resolution function is obtained from line profiles given by a fine quartz powder and its contribution to line broadening is subtracted. From these corrected WAXS spectra, one calculates the mean dimensions and orientation of the crystallites.

The peaks integral is proportional to the sample crystallinity; a precise conversion into absolute crystallinity necessitates lengthy and careful procedures that were not presently employed.[53] In this work, the crystallinity χ is determined using the simplified method of Mitchell.[4] From the scattered intensity of the amorphous phase (halo centered at $s = 13.5$ nm^{-1}), in semicrystalline material $I_a^*(s)$ at each temperature and in completely amorphous material $I_a(s)$ (just above T_m), one deduces the crystallinity $\chi = (I_a - I_a^*)/I_a 100$. Similar methods have been applied by Dumbleton and Bowles,[54] by Lee et al.[55] and by Trabelsi et al.[56] for determining the crystallinity around a crack tip in natural rubber.

In cyclic deformation, this method cannot be used directly; therefore, one has measured the normalized intensity I_{002}. Knowing the relation between χ and I_{002} at each temperature and draw ratio in static deformation (see Figure 3a of ref 56), we determined χ (%) during stretching and recovery at room temperature. For $N_C = 335,$ 238, *145* at 23 °C and for $\lambda_{max} = 5-6$, the maximum crystallinities are, respectively, as follows: $\chi_{max} = 25, 15, 10\%$.

The crystallite sizes $\langle l_{hkl}\rangle$ in the direction normal to the (*hkl*) planes are deduced from the Scherrer formula:

$$\langle l_{hkl}\rangle = K\lambda/(\beta_{1/2} \cos\theta) \quad (1)$$

Here $\beta_{1/2}$ is the reflection angular half-width, λ the radiation
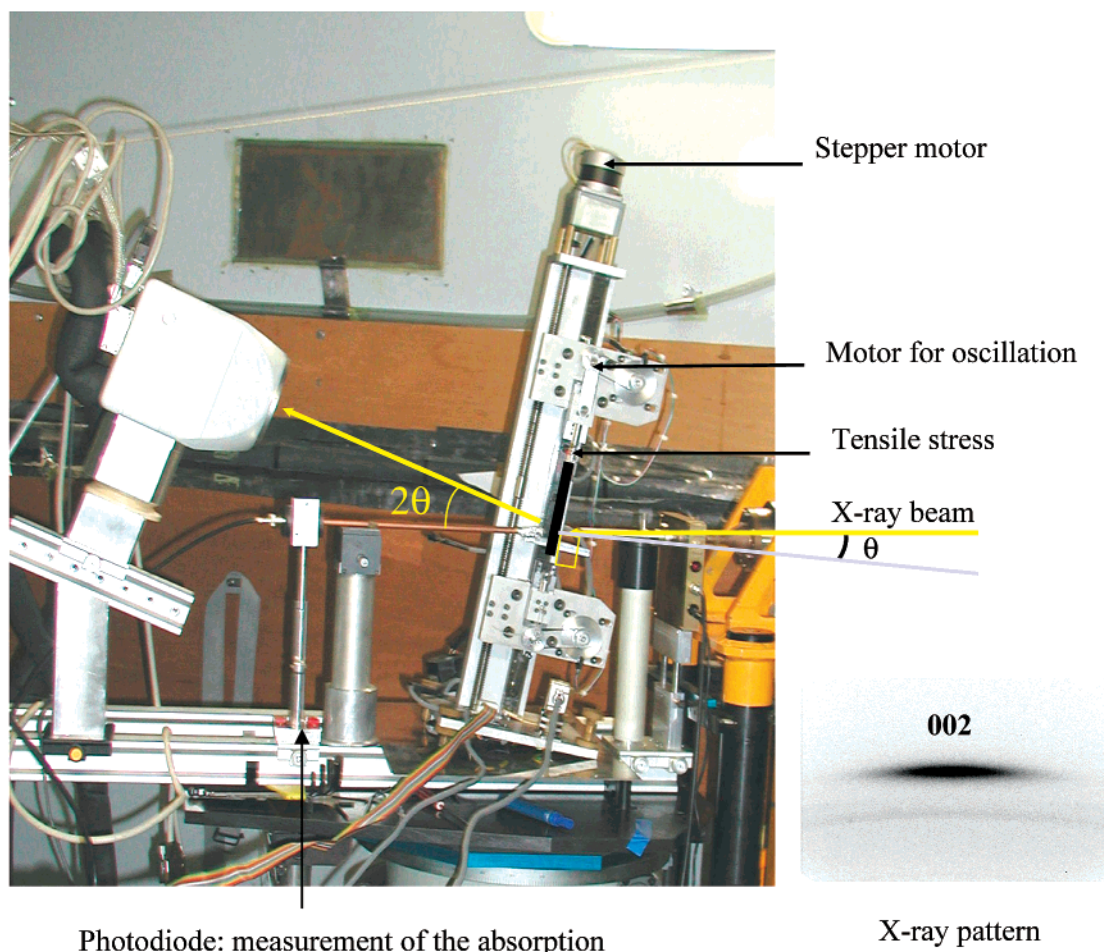
Figure 1. Experimental setup for dynamic mechanical and WAXS measurements at the Synchrotron source (Lure). The drawing machine is titled by an angle 10° to observe the 002 reflection. The CCD camera is on the left side. A photodiode after the sample measures the absorption of the X-ray beam. In insert, (on the right side), a typical image of the meridian 002 reflection of natural rubber is displayed.

wavelength (0.1542 nm), and θ the Bragg angle; K is a constant that depends on such factors as the crystallite shape or size distribution and which is usually close to unity.[50,57] A value of 0.78 was presently chosen in view of simulations of experimental profiles based on parallelepipedic crystallites and log-normal size distributions.

The crystallite orientation along the draw axis is deduced from the azimuthal profile of the reflection.[58,59] Experimental profiles are well-adjusted by Gaussian functions and can be fully characterized by their half-width at half-height $\delta\psi_{1/2}$; the parameter $\langle\cos^2\psi\rangle$ is used in other publications.[36,53]

3. Morphology during Static Deformation

3.1. Crystallization. (a) Crystallites Sizes during Crystallization. Figure 2a shows the variation of the crystallinity χ and the tensile stress σ as a function of the crystallization time. Sample **II** ($N_C = 238$) has been drawn at $\lambda = 3$ at 80 °C, then quenched to $T_C = -25$ °C, at this temperature the applied stress is σ_0. At short times $t < t_0$, $\chi = 0$ and $\sigma = \sigma_0$ is constant, the process of crystallization begins after the incubation time t_0, for longer times χ and σ vary in an opposite manner. At the end of the process, the crystallinity reaches a value $\chi_{max} = 25\%$ and the stress a value $\sigma_m \sim \sigma_0/4$. The inflection points of the curves $\chi(t)$ and $\sigma(t)$ define the same half time $t_{1/2}$ of crystallization. Similar curves are obtained for the others samples ($N_C = 145, 335$) drawn below $\lambda < 4$. This correlation between the crystallinity

and the stress relaxation has been described by Gent for different kind of rubbers, and the crystallinity was measured by dilatometry.[18,22,23]

For sample **II** (-25 °C, $\lambda = 3$, $N_C = 238$) complete crystallization occurs in 30 h, and this slow crystallization enables us to measure with accuracy the crystallites sizes during isothermal crystallization process, in particular at the beginning, near the incubation time. Such study on highly drawn samples is not possible for $\lambda > 5$ as the incubation time (and the half time $t_{1/2}$) becomes shorter than the time necessary to reach the thermal equilibrium during quenching.

Figure 2b gives the values of the crystal sizes along the three different directions (200), (120), (002) vs the crystallization time. The most important feature, which should be remarked, is the fact that all these dimensions do not vary with time meanwhile the crystallinity increases up to 25%. One concludes that the crystallites do not thicken and do not rearrange to form lamellae or other type of arrangements during crystallization; the increase of crystallinity is due to the increase of the number of crystallites having constant sizes.

In vulcanized rubber crystallized at high supercooling (for the sample of the figure, $N_C = 238$, $\Delta T = 50$ °C, $T_C = -25$ °C, $T_m = 25$ °C, $\lambda = 3$) the dimension $l_C = l_{002}$ along the drawn direction is about 50 Å, which is typically the stem length of quenched homopolymer PE, PET, etc, crystallized at high supercooling.[42,60] In these
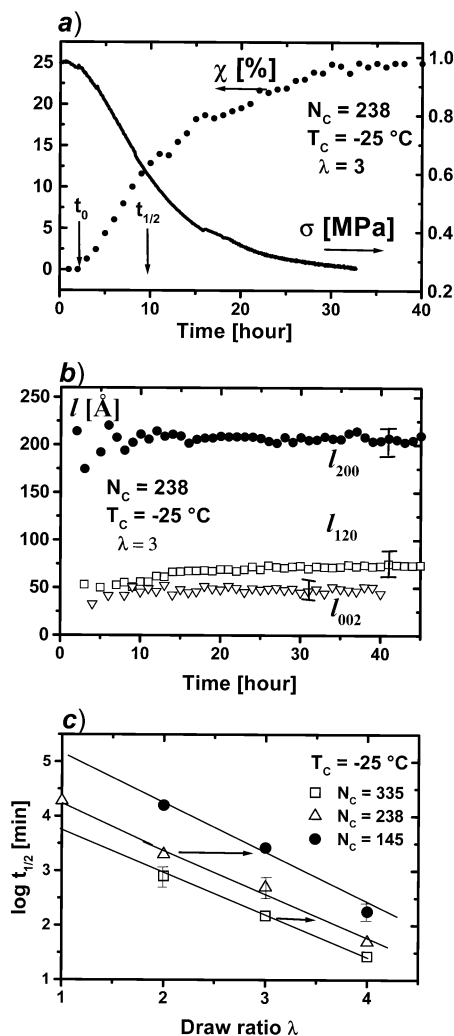
Figure 2. Crystallization of drawn NR sample **II** (N_C = 238 monomers) at λ = 3 and T_C = −25 °C. (a, b) Variation of the crystallinity, tensile stress and crystallites dimensions l_{200}, l_{120}, and l_{002}. (c) Half time of crystallization $t_{1/2}$ of vulcanized natural rubbers as a function of draw ratio and number of monomers (N_C = 145, 238, and 335) between two cross-links.

un-cross-linked polymers it is well-known that during isothermal crystallization the crystallites formed at the beginning of the process agglomerate laterally to form crystalline lamella of constant thickness. This process of rearrangement from globular to lamellar structure (small crystallites to large crystalline lamellae) has been observed by electron microscopy techniques on poly-olefins see for example the book of Strobl[43] and on non-cross-linked rubbers by Luch and Yeh.[15] From the work of these last authors one concludes that the process of crystallization of un-cross-linked rubber and other polymers (polyolefine, polyamide, polyesther) are not different. The small-angle X-ray scattering (SAXS) of stretched samples (N_C = 145, 238, and 335) at room temperature shows no interference peak, and this suggests that the morphology is irregular in all the directions of the sample and that no lamellar periodicity can be defined in these vulcanized samples. By electron microscopy, more or less regular periodic lamellar and shish-kebab structures have been observed only in un-cross-linked rubber.[15,17] In conclusion the cross-links in vulcanized rubber must be considered as obstacles for the molecular rearrangements which are necessary during and/or after crystallization, for transforming the

disorder structure (the so-called granulate structure of Strobl) at the beginning of the crystallization into a one-dimensional lamellar structure after complete crystallization (after annealing).

In Figure 2c the half time of crystallization $t_{1/2}$ at −25 °C is reported as a function of draw ratio and number N_C of monomers between cross-links. It is found that log $t_{1/2}$ decreases linearly with draw ratio:

$$\log t_{1/2} = A_t(N_C) - B_t\lambda; \quad B_t = 1.1; \quad 1 < \lambda < 4 \quad (2)$$

Gent[18,23] found a similar law for two natural rubbers (NR) vulcanized with sulfur, N_C = 110 and 152, drawn below λ = 3, in butadiene rubber[18a] (BR), cross-linked with 0.15 and 3% DCP drawn at −15 °C, and in *trans*-polychloroprene[18c] (TPC) at different crystallization temperatures (in this last material the curves log $t_{1/2}(\lambda)$ present a certain curvature). The slope B_t for the NR, BR and TPC samples is constant $1.1 > B_t > 1$ and does not seem to vary with temperature. This behavior has not been discussed in detail in the literature. Here we report similar results but in a somewhat large domain of extension, λ < 4.5. The slope B_t is constant for the three vulcanized rubbers and is equal to the value reported by Gent for the different rubbers. When the number of monomers N_C between cross-links decreases from 335 to 145 the curve log $t_{1/2}$ is shifted toward high draw ratio, by a factor $\Delta\lambda$ on the order of 1−1.3. The same shift factor will be reported for the melting temperature, when N_C is changed. Finally one has to remark that cross-links are comparable to the defects or non-crystallizable comonomers (or solvent) along the chains, which decrease the melting temperature of the polymer and consequently slow-down the kinetics of crystallization (at fixed temperature). The effect of the cross-link density on the crystallite sizes is analyzed in the following part.

(b) Crystallite Sizes after Complete Crystallization. Parts a−c of Figure 3 give the crystallites dimensions as a function of draw ratio λ and number N_C of isoprene monomers between cross-links; see Table 1 to know the correspondence between N_C and the mass of suphur per 100 g of rubber. The samples (N_C = 145, 238, and 335) have been drawn at high temperature (80 °C) and then quenched at −25 °C. All the measurements have been done at equilibrium at −25 °C after complete crystallization, that is to say when the WAXS intensity and the relaxation force level off. From this figure one concludes that

(a) The dimensions l_{200} and l_{120} decrease by a factor of 2 when λ increases from 3−5 and then levels off. By transmission electron microscopy, Shimizu[17] observed in non-vulcanized natural rubber (under the same conditions) a decrease of the average length of the lamellae perpendicular to the stretching direction with increasing strain.

(b) The dimension l_{002} parallel to the draw ratio increases with λ.

(c) All the dimensions l_{200}, l_{120} and l_{002} decrease with the cross-link density, this effect becomes more important for l_{200} and l_{120} when the draw ratio increases above λ = 4.

In Figure 3d the volume $V_C = l_{200}l_{120}l_{002}$ which is proportional to the crystallite volume $V_{crystal} = V_C \cos \alpha$, is plotted vs the draw ratio. The angle α between the directions of the (020) and (120) planes is 70°. From this figure, one concludes that the mean volume of the
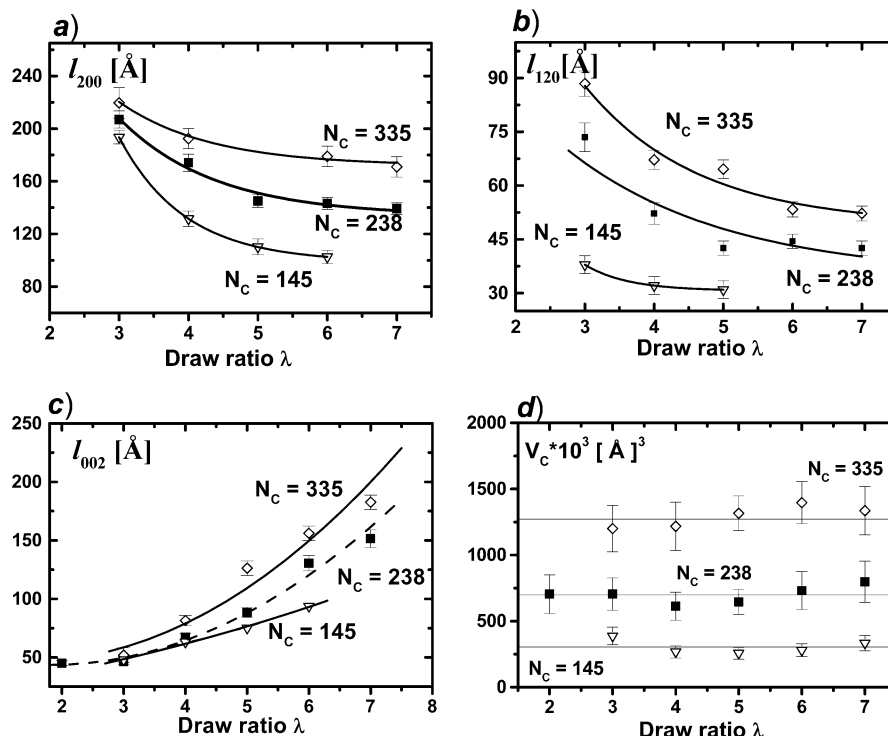
Figure 3. Crystallites dimensions l_{200}, l_{120}, and l_{002} (a, b, c) and crystallites volume V_C (d) as a function of draw ratio λ for the three different cross-linked samples NR (N_C = 145, 238, and 335) crystallized at $T_C = -25$ °C.

crystallites formed at -25 °C ($\lambda < 5$) or during quenching ($\lambda \geq 5$) is independent of λ, and decreases when the density of cross-links increases. When the number of monomers between cross-links decreases by a factor of 2.3, the volume decreases by a factor of 3. For the less vulcanized rubber N_C = 335, a small increase with λ is however noted. The effect of cross-links on three sizes is evident; cross-links decreases the mobility of the chains, impedes the rearrangement of the crystallites, limits the final extent of crystallinity and crystallites size, and therefore decreases the crystallite volume.

The first question which should be asked is the following: Is the crystallization still isothermal in all these drawn and quenched samples? Göritz et al.[19] distinguish two kinds of crystallization: stress-induced crystallization and temperature-induced crystallization, corresponding here respectively to nonisothermal and isothermal crystallization.

For vulcanized rubber of similar composition (with 2.25 g of sulfur) Mitchell and Meier,[25] using a high-speed tester instrument at room temperature, found that for $\lambda = 5-6$ crystallization occurs in about 60 ms. In our samples (N_C = 145, 238, and 335, drawn above λ = 5), the incubation time t_0 and the half time $t_{1/2}$ of crystallization cannot be determined by the WAXS method. The first WAXS measurement, 3 min after thermal stabilization, shows that the crystallinity had attained its equilibrium value. Below $\lambda = 4.5$, WAXS measurement shows that crystallization occurs after the thermal equilibrium. One recalls here that the thermal diffusivity of polymers is about $a = 10^{-3}$ cm²/s; therefore, the quenched samples of thickness 1 mm studied here reaches the thermal equilibrium in a time on the order of $t_e = e^2/a \sim 10$ s. The results of Mitchell and Meier[25] and ours show that crystallization in the quenched samples drawn above $\lambda = 5$ is nonisothermal. The appearance of the plateau above $\lambda = 5$ in Figure 3a,b seems to correspond to this change of regime. It would
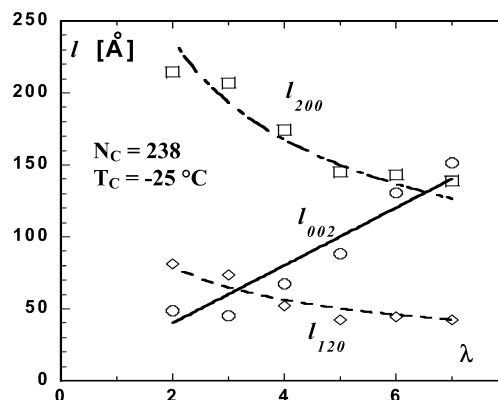

Figure 4. Variation of the crystallite sizes l_{200}, l_{120}, and l_{002} with draw ratio of sample **II** (N_C = 238) at -25 °C. Lines are the best fits with the affine deformation laws (relation 3a).

be interesting to know why in this new regime of crystallization the sizes l_{200} and l_{120} level off, whereas the crystallite size l_{002} is still increasing with λ.

In Figure 3d, it is important to remark that the change of regimes of crystallization when λ increases does not involve any conspicuous change in the crystallite volume observed at -25 °C, whatever is the degree of cross-links. The new effect reported in this figure is to our opinion related to the affine deformation of the chains before crystallization or of the crystallites when nucleation occurs.

In Figure 4, the data of sample **II** (N_C = 238) at -25 °C are fitted with the affine deformation laws for $\lambda \geq 3$:

$$l_{200} = l_{200}^0 \lambda, \quad l_{120} = l_{120}^0 \lambda^{0.5}, \quad l_{002} = l_{002}^0 \lambda^{0.5} \quad (3a)$$

The extrapolated crystallite sizes l_{hkl}^0 for $\lambda = 1$ and the correlation factors R_{hkl} of the fits are given in Table 2. One has remarked that below $\lambda = 3$ the crystallite sizes

Table 2

l_{hkl}^{0} (Å)	$l_{200}^{0} = 335$	$l_{120}^{0} = 112$	$l_{002}^{0} = 20$
R_{hkl}	$R_{200} = 0.92$	$R_{120} = 0.94$	$R_{002} = 0.96$

remain constant. The change of behavior at this draw ratio seems to correspond to the transition from lamellar to fibrillar morphologies observed by some authors.[14,17,18a]

In the isotropic supercooled melt the unperturbed dimension[61] r_C of a *cis*-polyisoprene chain having N_C monomers is $r_C = 0.8 \sqrt{M_C} \sim 6 \sqrt{N_C}$ (in Å), with $M_C = N_C M_0$, the molecular weight of a monomer being $M_0 = 64$. The volume around a cross-link is then $V \sim (4\pi/3)*(rc)^3 \sim 860 N_C^{1.5}$ (Å^3) which deforms in a affine manner ($V = $ constant). Figures 3 and 4 tell us that, in this deformed region, the crystallites undergo the same type of deformation. The crystallites volume V_C (Figure 3d) and the calculated values of V verify for $145 \leq N_C \leq 335$ the following linear law:

$$V_C \sim 0.25 * V, \quad R = 0.999 \qquad (3b)$$

This experimental law and the good correlation factor, R, observed lead to the following important conclusion:

The crystallites and the mesh of the cross-links have the same order of sizes and then deform in affine manner. V_C is constant and is about the volume per cross-link.

Obviously this law is not valid at low and high values of N_C. Crystallization is limited by the cross-link density for high value of N_C and by the entanglements for low values of N_C as was suggested in un-cross-linked polymers.[45]

One wonders if the increase of the crystallite size $l_C = l_{002}$ with λ is a consequence of the change of the supercooling as it would be predicted by the secondary nucleation theories[42,43] or by the model of crystallite annealing and thickening appearing during crystallization.[46] In these models without going into details, the crystallite size varies inversely with the degree of supercooling, $\Delta T = T_m - T_C$; the Lauritzen and Hoffman law, $l_C \sim 1/\Delta T(\lambda)$, is in fact observed only in a small domain of crystallization temperature below T_m. The width of this domain where l_C is constant depends on the nature of the chains; for example in branched polyethylene and cross-linked chains the variation of l_C with temperature is weaker than in linear polyethylene.[44] It must be noted also that, for most polymers,[60] l_C is found to be constant when the supercooling is greater than 20 °C. In natural rubbers Luch and Yeh[15] reported very small variations of the thickness l_{002} of the crystalline lamellae with the crystallization temperature, this is confirmed by ours WAXS data discussed hereafter. For $\lambda > 4$, in vulcanized rubbers, crystallization is nonisothermal, therefore one cannot estimate ΔT. For $\lambda < 4$, crystallization at $T_C = -25$ °C is isothermal, the crystallites sizes $l_{002} = l_C$ for $\lambda = 2$ and 4 are respectively 40 Å and 60 Å for $N_C = 238$ (see Figure 3c). The corresponding melting temperatures are $T_m = 0$ °C and 60 °C (see Figure 6a). As the crystallization temperature is $T_C = -25$ °C, the corresponding supercooling $\Delta T = T_m - T_C$ is respectively 25 and 75 °C. Therefore, one concludes that l_C cannot be derived from the Lauritzen and Hoffman law $l_C \sim 1/\Delta T(\lambda)$.

3.2. Melting of Drawn Samples. (a) Crystallinity and Melting Temperature. Figure 5a gives the crystallinity of sample **II** ($N_C = 238$) drawn at $\lambda = 6$ as a function of temperature. The sample has been drawn
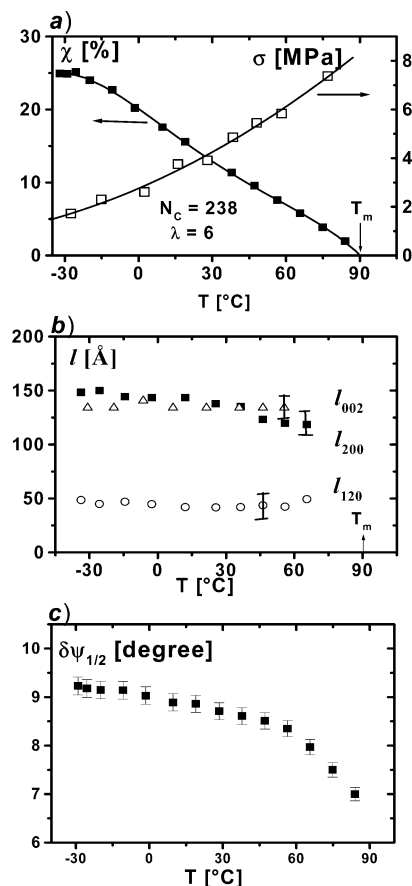

Figure 5. Melting process for the drawn sample **II** ($N_C = 238$ monomers) at fixed draw ratio $\lambda = 6$, crystallized at $T_C = -25$ °C. Crystallinity χ and the tensile stress σ (a), crystallites dimensions l_{200}, l_{120} and l_{002} (b), and orientation $\delta\psi_{1/2}$ along stretching direction 001 (c). Heating rate is 0.5 °C/min.

above the melting temperature (90 °C) to erase the thermal history,[34] then quenched at −25 °C and annealed at that temperature to obtain complete crystallization. The sample is heated by steps of 5 °C up to the complete melting. At each temperature when the tensile stress stabilizes (at the equilibrium state), the WAXS intensity is recorded and then the crystallinity is determined. From this figure one concludes that the melting process is progressive; between −25 and +90 °C crystallinity χ and stress σ vary linearly with T, in an opposite manner. The melting temperature $T_m = 90$ °C is obtained by extrapolating the crystallinity curve (see arrow in Figure 5a). During crystallization at −25 °C, the stress and therefore the amorphous chains relax partially. During heating the stress increases gradually, indicating that the amorphous chains become more and more stretched. T_m must be considered as the melting temperature of the last crystallite in equilibrium with the drawn amorphous chains. At this melting temperature the local draw ratio of the amorphous chains becomes equal to the macroscopic draw ratio. Between −25 °C and T_m, the crystallites are still in equilibrium with the stretched amorphous chains but the local and macroscopic draw ratios are different. In Figure 5b,c it is shown that during progressive melting the morphology (crystallite sizes and orientation) does not change conspicuously. This behavior is very analogous to what is observed during crystallization (see Figure 2a,b). From Figures 2 and 5, one concludes that melting and crystallization proceed by formation and disappearance
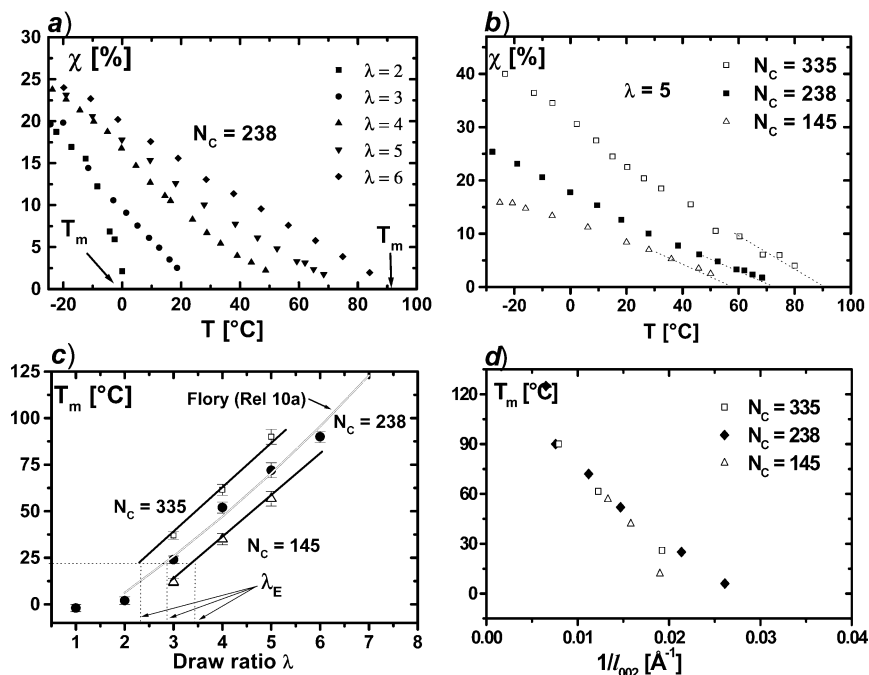
Figure 6. (a) Crystallinity χ as a function of draw ratio λ and temperature for drawn NR sample **II** (N_C = 238 monomers) at 2 $\leq \lambda \leq$ 6 and crystallized at $T_C = -25$ °C. (b) Crystallinity as a function of temperature at fixed draw ratio λ = 5 for the three different NR cross-linked samples (N_C = 145, 238, and 335) crystallized at $T_C = -25$ °C. (c, d) Melting temperature T_m in °C as a function of draw ratio (c) and as a function of the inverse of crystallites dimensions $1/l_{002}$ (d) for the three different cross-linked samples (N_C = 145, 238, and 335) crystallized at $T_C = -25$ °C.

of crystallites of constant dimensions. These results are found for all the samples **I**, **II**, and **III** (N_C = 145, 238, and 335) whatever is the draw ratio.

In Figure 6a the melting curves $\chi(T)$ of the samples **II** (N_C = 238) drawn at different ratios (1 < λ < 7) are given. $\chi(T)$ can be approximated by the linear relation:

$$\chi = \chi_{max}\left(\frac{T_m - T}{T_m - T_0}\right), \quad T_0 = -25 \text{ °C}; \quad \chi_{max} = 0.25 \quad (4)$$

At $T_0 = -25$ °C the maximum crystallinity χ_{max} is on the order of 25% and does not vary much with the draw ratio, while below $T_0 = -25$ °C, the crystallinity is found to be constant. It is important to remark that the melting behavior is the same for isothermally (λ < 4.5) and non isothermally (λ > 4.5) crystallized samples, but the melting temperature T_m of the last crystallites increases with λ (see arrows in Figure 6a). Taylor et al.[10] found the same effect in polybutadiene; the crystallinity at -35 °C varies from 20 to 26% when the draw ratio increases from 2.2 to 7.7. Equation 4 applies also for the other samples, where the maximum crystallinity χ_{max} is function of N_C.

In Figure 6b, one compares the melting curves of the three vulcanized samples drawn at λ = 5. As expected, the crystallinity and the melting temperatures of these materials, crystallized in the same conditions at -25 °C, decrease with the cross-link density ($\nu \sim 1/N_C$). Alexander et al.[2] and Taylor et al.[10] using, respectively, X-ray scattering and birefringence found similar linear law for drawn polybutadiene. From this figure one finds that the maximum crystallinity χ_{max} obtained at -25 °C as a function of N_C, is given by the following empirical law:

$$\chi_{max}(\%) = -4.8 + 0.13 \, N_C; \quad 335 \geq N_C \geq 145 \quad (5)$$

At higher temperature one finds similar relations, the slope $d\chi/dN_C$ being a constant.

From Figure 6a,b one concludes that χ/χ_{max} vs T/T_m is a master curve, independent of λ and N_C.

It would be interesting to verify if these relations 4 and 5 applies for higher values of N_C when N_C is about the number of monomers between entanglements (in particular in un-cross-linked rubbers).

In Figure 6c the melting temperature T_m is reported as a function of λ and N_C. The melting temperature deduced from the $\chi(T)$ curves increases linearly with draw ratio, this is a well-known result.[18,20,22,23] In general, the melting temperature, found in the literature, is deduced from the stress curves[22] or from dilatometry.[19,21] The role of the cross-link density reported here is new; T_m can be put in the linear form.

$$T_m = T_m^0(N_C) + B_T(\lambda - 1); \quad B_T = 32 \text{ °C}, \quad \text{for } \lambda > 3 \quad (6)$$

The constant $T_m^0(N_C)$ obtained by extrapolation (λ = 1) decreases with N_C and does not coincide with the melting temperature of the isotropic NR. The slope B_T = $dT_m/d\lambda \sim 32$ °C varies weakly with N_C and is about the value found by Gent et al. (B_T = 48 °C, see fig. 5 of ref.22), in the domain of deformation, λ > 2.5, for natural and synthetic rubbers cross-linked with 1% DCP. These authors observed that T_m is constant (-5 °C) for λ < 2.5. As reported in Figure 6c for N_C = 238, we have found that T_m is also constant for λ < 3. It has been observed by many authors[14,17,18] at λ = 3, a transition from spherulitic to fibrillar growth. In our case, as shown by Figure 4, the crystallites sizes are found constant below λ = 3. This change in the regime of crystallization can explain why the melting temperature is constant for λ < 3.

When the number N_C decreases from 335 to 145 the curve $T_m(\lambda)$ is shifted toward a high draw ratio by a

factor $\Delta\lambda$ on the order of $1-1.1$. For the same samples ($N_C = 145$, 238, and 335), the curve $\log t_{1/2}(\lambda)$, giving the half time of crystallization vs λ, is shifted by the same amount, $\Delta\lambda \sim 1-1.1$ (Figure 2c). One concludes that the dependences of $\log t_{1/2}(\lambda)$ and $T_m(\lambda)$ with draw ratio (and with N_C) have the same origin. This can be explained simply by the model of thermal activated motions. The chains crystallize at a rate which is given by the Arrhenius law:

$$\log \nu \sim \log t_{1/2} \sim E/RT - E/RT_m \sim (E/RT_m^2)(T_m - T) \quad (7a)$$

If T is far from T_m and approaches to the T_g value, one should write the WLF equation, but this will not change our discussion. To our knowledge, the experimental relationship between the activation energy E of the crystallites growth rate and the draw ratio has not been studied. If one assumes that E is weakly dependent on λ, relations 6 and 7a lead to the observed linear relation $\log t_{1/2} \sim \lambda$ given in relation 2.

$$\log t_{1/2} \sim -\frac{E}{RT_m^2}B_T\lambda; \quad \frac{E}{RT_m^2}B_T = B_t \quad (7b)$$

(b) Relationship between Melting Temperature and Crystallite Size l_{002}. In Figure 6d the melting temperature T_m is plotted as a function of the inverse of the crystallite size l_{002}. T_m and l_{002} are measured at -25 °C respectively from Figure 3c and 6c. As discussed hereafter during heating (up to the melting) a small increase of l_{002} is noted. In the domain 40 Å $< l_{002} <$ 200 Å the figure shows that the melting temperature follows the linear law:

$$T_m = T_m^*\left[1 - \frac{\beta}{l_{002}}\right]; \quad \beta = 5.3 \text{ Å} \quad (8)$$

This relation, 8, has the same form as the Thomson relation. The characteristic length $\beta = 5.3$ Å is typically the Thomson length observed in small molecules and polymers crystallized in the isotropic state: for PE, PEO, paraffin, and benzyl alcohol, this length is respectively[62] 10, 5, 3.7, and 8.3 Å. Dalal et al.[63] verified the Thomson law in natural non-vulcanized rubber in the isotropic state; they found a Thomson length on the order of 8 Å and a melting temperature $T_m^* = 33$ °C, for crystallites of infinite length. Our results show that the characteristic length β in relation 8 is not dependent on the cross-link density. The existence of the master curve $T_m (1/l_{002})$ is puzzling. The decrease of N_C at constant draw ratio involves a simultaneous decrease of the T_m and l_{002} values. The apparent simplicity of the above Thomson relation observed in drawn materials should not hide that the physical origin of this law is not totally understood; in particular, one has to explain the origin and the meaning of the extrapolated characteristic temperature $T_m^* = 120$ °C. Is it the melting temperature of crystallites with infinite thickness obtained in highly drawn sample, $\lambda^* \sim 7-8$, as seen in Figure 6c? Is this extrapolated draw ratio λ^* (before the rupture of sample) of the same order of the maximum draw ratio, $\lambda \sim \sqrt{N_C}$ expected when the network chains are nearly totally extended?

(c) Relation between Crystallinity and Stress. During heating the stress increases as predicted by the
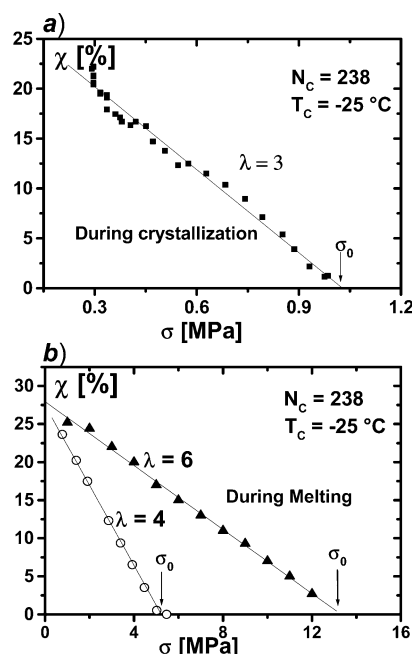

Figure 7. Crystallinity χ as a function of the tensile stress σ for drawn NR sample **II** ($N_C = 238$) at $\lambda = 3$ during crystallization at $T_C = -25$ °C (a) and at $\lambda = 4$ and 6 during melting (b).

Flory model[34] and observed by various authors.[37] This effect is opposite to what is observed during crystallization. One reports in Figure 7a the variations of the crystallinity χ vs the stress σ during crystallization at -25 °C for drawn sample **II** ($N_C = 238$, $\lambda = 3$), the data are deduced from Figure 2a. In Figure 7b, one gives the same curves $\chi(\sigma)$ for the same sample drawn at $\lambda = 4$ and 6 but during progressive melting from -25 °C to T_m. Obviously, at the end of melting the force applied to the sample is equal to the tensile stress of the sample before crystallization (before quenching). The measurements have been done at equilibrium during melting (Figure 7b) and not at equilibrium during crystallization (Figure 7a). During both processes $\chi(\sigma)$ can be put on the linear form:

$$\chi = \chi_{max}\left(1 - \frac{\sigma}{\sigma_0}\right)\% \pm 5\%, \quad \chi_{max} = 25\% \text{ for } N_C = 238 \quad (9)$$

In Figure 7a, σ_0 is the applied stress on the noncrystalline sample at -25 °C, where the crysallinity χ is equal to zero. In Figure 7b, σ_0 is the stress at T_m after complete melting. One finds similar laws for the other samples ($N_C = 335$, 145) where the crystallinity χ_{max} is different and given by Figure 6b. In all the situations, out or in equilibrium, $(\chi/\chi_{max})((\sigma/\sigma_0))$ is a master curve, which does not depend on the draw ratio. It must be noted that at low temperature (at equilibrium) the crystallinity of sample **II** is always on the order of 25 % and the stress has not relaxed to zero but to a minimum value σ_{min}, which is much less than the applied stress, $\sigma_{min} \sim {}^1/_4\sigma_0$; this partial relaxation has been observed by various authors.

3.3. Relation with the Flory Model. In this model, it is assumed that all network chains are Gaussian and pass through a crystallite; the free energy is only function of crystallinity and draw ratio. This model predicts neither the thickness of the crystallites l_C nor

the mean distance L between crystallites. Minimization of the free energy gives the following:

$$\frac{1}{T_m^0} - \frac{1}{T_m} = \frac{R}{\Delta H_m}\varphi(\lambda); \quad \lambda > 1 \qquad (10a)$$

$$\chi = \frac{\sigma_0 - \sigma}{\sigma_0\left(\dfrac{6N_C}{\pi}\right)^{1/2}\left[\lambda - \left(\dfrac{1}{\lambda^2}\right)\right]^{-1} - \sigma} \qquad (10b)$$

$$\varphi(\lambda) = \left(\frac{6}{\pi N_C}\right)^{1/2}\lambda - \frac{\lambda^2}{2N_C} - \frac{1}{\lambda N_C} \qquad (10c)$$

Here ΔH_m, the melting enthalpy, is assumed to be independent of temperature and draw ratio, and σ_0 is the applied stress before crystallization. Modifications of this model have been given by various authors[35,37,38] taking into account the non-Gaussian character of the chains at high extension, the fact that the chains can be folded, and the fact that the crystallites are not perfectly oriented along the stretching direction. In all these theories "à la Flory", ΔH_m is assumed to be constant and no prediction is done about the dependency of the crystallite sizes with T and λ.

In Figure 6c, one reports the fit for $\lambda > 2$ of the experimental curve $T_m(\lambda)$ of sample **II** ($N_C = 238$) with relation 10a. The correlation factor is $R = 0.991$ and the fit parameters are as follows: $\Delta H_m = 2700$ J/mol and $N_C = 213$ instead of $\Delta H_m = 4700$ J/mol and $N_C = 238$. In this particular case, the second and third terms of $\varphi(\lambda)$ in relation 10c are negligible and relation 10a becomes

$$\frac{1}{T_m^0} - \frac{1}{T_m} \approx \frac{R}{\Delta H_m}\left(\frac{6}{\pi N_C}\right)^{1/2}\lambda \approx 11.36\frac{\lambda}{\Delta H_m\sqrt{N_C}};$$

$$\Delta H_m \text{ in J/mol} \quad (11)$$

The above relation predicts that the slope $dT_m/d\lambda \sim 1/\sqrt{N_C}$ should increases when N_C decreases from 335 to 145. As shown by Figure 6c, this is not observed.

Finally, one has fitted the results of Figure 7a with the Flory relation (relation 10b), the fit parameter N_C is found to be $N_C = 64$ which is lower than the value $N_c = 238$ obtained by swelling measurements. As pointed out by Kim and Mandelkern,[20] in most cases of interest, in particular in cases of Figure 7, relation 10b leads to $\chi = K[1 - \sigma/\sigma_0]$ with $K = (\pi/6N_C)(\lambda - 1/\lambda^2)$. Again the predictions of Flory are in contradiction with the experimental law, relation 9, where K is not dependent on draw ratio.

In conclusion, the Flory model gives acceptable values for ΔH_m and N_C when the variations of T_m with λ are considered. However, this model does not predict the observed relationship (relation 9) between χ and σ and the fact that the crystallinity at low temperature is independent of draw ratio. Again, here we emphasize that this model does not give any information about the variations of the crystallite sizes with temperature, draw ratio, and cross-link density.

4. Morphology during Dynamic Deformation

Samples **I**, **II**, and **III** ($N_C = 335, 238, 145$) have been drawn at room temperature (23 °C) up to $\lambda_{max} \sim 6$ and then relaxed at the constant strain rate $\dot{\epsilon} = 1$ mm/min. Figure 8 gives the stress and the crystallinity vs λ as

explained in (section 2.2.c). Figure 9 gives the corresponding crystallite orientation $\delta\psi_{1/2}$ and size l_{002} along the stretching direction vs λ. One discusses in the following the deformation processes occurring during stretching and recovery.

4.1. Stretching. When the draw ratio increases above $\lambda = 3$, the stress strain curve begins to deviate from the curve predicted by the rubber elasticity theory.[31] In Figures 8 and 9 crystallization appears at point A, $\lambda_A = 4$. In samples **I** and **II** ($N_C = 335, 238$), the tensile stress seems to be constant up to point B, $\lambda_B = 5$. The stress releases partially with time (about 20%) if the sample is kept at a fixed draw between λ_A and λ_B. In this domain the crystallinity increases linearly with draw ratio. These effects observed in different samples confirm that the semicrystalline phase in this region is not in equilibrium. The plateau of the strain stress curve can be due to two antagonist effects of similar amplitude: the relaxation of the amorphous chains during crystallization and the formation of new crystallites which act as new cross-links and then tend to increase the stress. This last effect was pointed out by Flory[34] in his early work in 1947.

Toki et al.[47] on similar cross-linked rubbers, found that crystallization starts at $\lambda_A > 4$ and that relaxation occurs (a decrease of 20% of the stress) if the sample deformation is stopped. However they did not observed the plateau AB described here and they reported higher values for λ_A. It is found in our sample that when the stain rate increases by a factor of 90, this draw ratio is shifted to $\lambda_A = 4.5$. In our opinion, these two effects are due to the higher strain rate used by these authors,[47,48] $\dot{\epsilon} = 50$ mm/min, instead of 1 mm/min in our work. As noted above the effect of increasing the strain rate $\dot{\epsilon}$ increases λ_A and decreases the length of the plateau AB. In conclusion from our work and others, the critical draw ratio λ_A for the onset of the crystallization is function of strain rate $\dot{\epsilon}$ and temperature[47] and not of cross-link density.

Above $\lambda_B = 5$ stress hardening occurs. The stress can be put on the quadratic form $\sigma \sim \lambda^2$ and the crystallinity χ increases linearly with draw ratio up to the maximum extension $\lambda_{max} = 5.5-6$.

It is important to remark that during stretching, the crystallite orientation and the crystal size l_{002} remain constant (Figure 9a,b). These data should be compared with the results obtained in condition of fixed extension at room temperature. Figure 10a gives the size l_{002} of these samples (**I**, **II**, **III**) in static deformation, for samples drawn at 90 °C ($4 < \lambda < 6.5$) and then quenched at 23 °C. The dimensions are systematically higher than obtained by crystallization at -25 °C, but the dependency of l_{002} with N_C is exactly the same. One remarks that the size l_{002} for $\lambda = 4$ in these static experiments corresponds to the values found during cyclic deformation (Figure 9b).

The same remark holds for the crystallite orientation $\delta\psi_{1/2}$; in Figure 10b, one compares this orientation for samples crystallized at -25 and $+23$ °C. It shows that the orientation depends only on λ and not the crystallization temperature and the cross-link density. From these observations one may conclude that during both crystallization processes (static and dynamic) the crystallites grow under very similar local extension of the amorphous chains.

Following the argument of Flory, one assumes that each new crystallite of constant volume, V_C, formed in
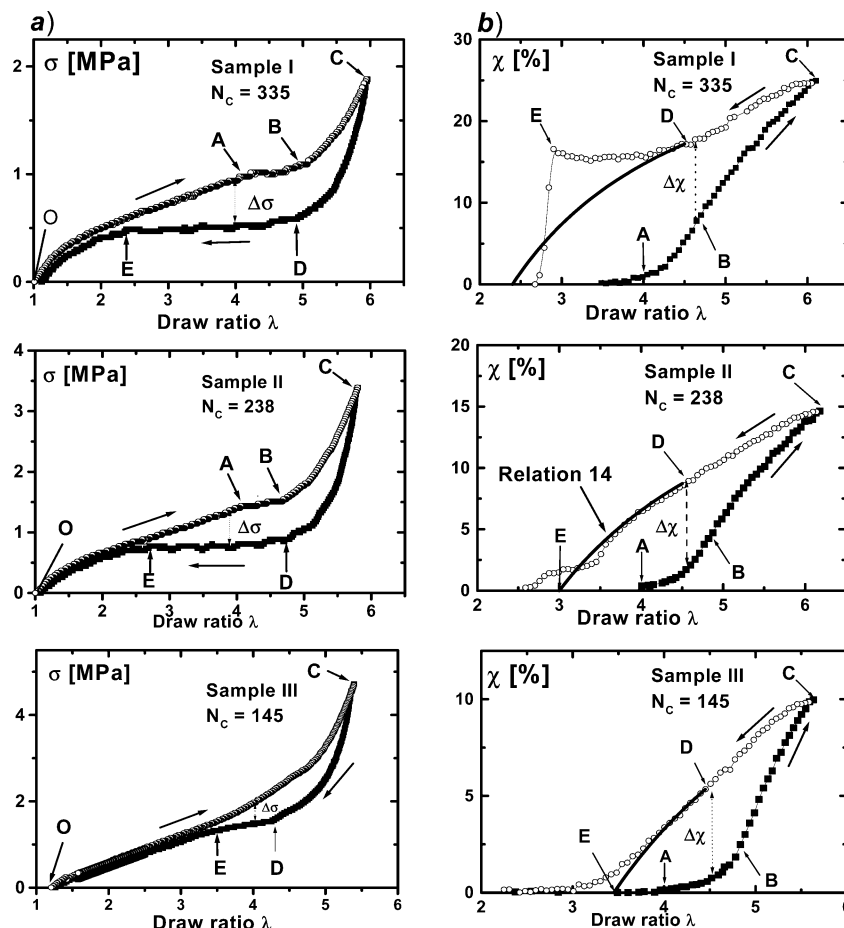
Figure 8. Stress-strain cycle (a) and crystallinity-strain cycles (b) with strain rate $\dot{\epsilon} = 1$ mm/min for the three different cross-linked NR samples ($N_C = 145$, 238, and 335) stretched at $T = +23$ °C. [OABC] and [CDEO] correspond respectively to the stretching and recovery curves indicated by arrows in the figure. In sample **I**, an inverse yielding effect appears (see Appendix). The heavy line in part b is the mean crystallinity deduced from relation 14.

this region acts as a cross-link. The density of cross-links is then the sum of the density of sulfur bridges ν_S and the density of crystallites $\nu_{cryst} = \chi / V_C$. The crystallinity varying linearly with λ as shown in Figure 8b and V_C being constant, the cross-link density is then

$$\nu = \nu_S + \nu_{cryst} \sim \chi / V_C \sim \lambda \tag{12}$$

Applying the rubber elasticity theory,[31] one obtains when the density of crystallites becomes greater than the density of sulfur cross-links:

$$\sigma \sim \nu_{cryst} KT(\lambda - 1/\lambda^2) \sim \lambda^2 \tag{13}$$

This is the trend observed in the stress-hardening region BC. In conclusion, stress hardening in vulcanized elastomers can be explained by the Flory argument without invoking the limitation of extensibility of the chains, and the curvature in the $\chi(\lambda)$ curve for $\lambda > 4.5$ is due to the increase in density of crystallites of constant morphology (same volume). Obviously the qualitative agreement between relation 13 and the experimental data does not preclude that the Langevin elasticity theory must be applied for large local deformation of the chains.

Finally, one emphasizes the similarity between the process of crystallization during stretching ($\lambda_A < \lambda < \lambda_{max}$) and the process of isothermal crystallization (Figure 2); both processes involve an increase of the number of crystallites with constant sizes.

4.2. Recovery. When the strain decreases at constant rate, the stress decreases abruptly curve CD in Figure 8a and then levels off for $\lambda_E < \lambda < \lambda_D$ (curve DE). The draw ratios λ_D and λ_B corresponding respectively to the appearance of the recovery curve plateau and the beginning of the stress hardening are of the same order of magnitude (see Figure 8a). This empirical law, $\lambda_D \approx \lambda_B \approx 4.8$ to 5.2, is clearly observed for samples **I** and **II**. For sample **III** ($N_C = 145$), the plateau DE of the stress strain curve is much less apparent, and the accuracy on λ_D and λ_B is about 0.5. The recovery plateau joints the traction curve at λ_E, and then recovery and traction curves merge together for $\lambda < \lambda_E$. The length DE of the plateau decreases with increasing cross-link density. From these recovery curves $\sigma(\lambda)$, the merging draw ratio λ_E can be estimated with an accuracy of ± 0.3. Toki et al.[48] did not observe this plateau during recovery; in our opinion this is due to the fact that their sample was highly cross-linked ($\nu_s = 1.2 \times 10^2$ mol/m³) compared to our sample **III** ($\nu_s = 0.94 \times 10^2$ mol/m³, $N_C = 145$) which presents a very small plateau.

During recovery, Figure 8b shows that crystallinity $\chi(\lambda)$ decreases linearly with λ, the recovery curve slope $d\chi(\lambda)/\delta\lambda$ is smaller than the stretching one. These results are at variance with the observations of Toki et al.[47] on rubbers vulcanized with 1.5 g of sulfur; these authors found that the crystallinity is still increasing at the beginning of the recovery, when the strain decreases from 600% to 575%. Also their crystallinity,
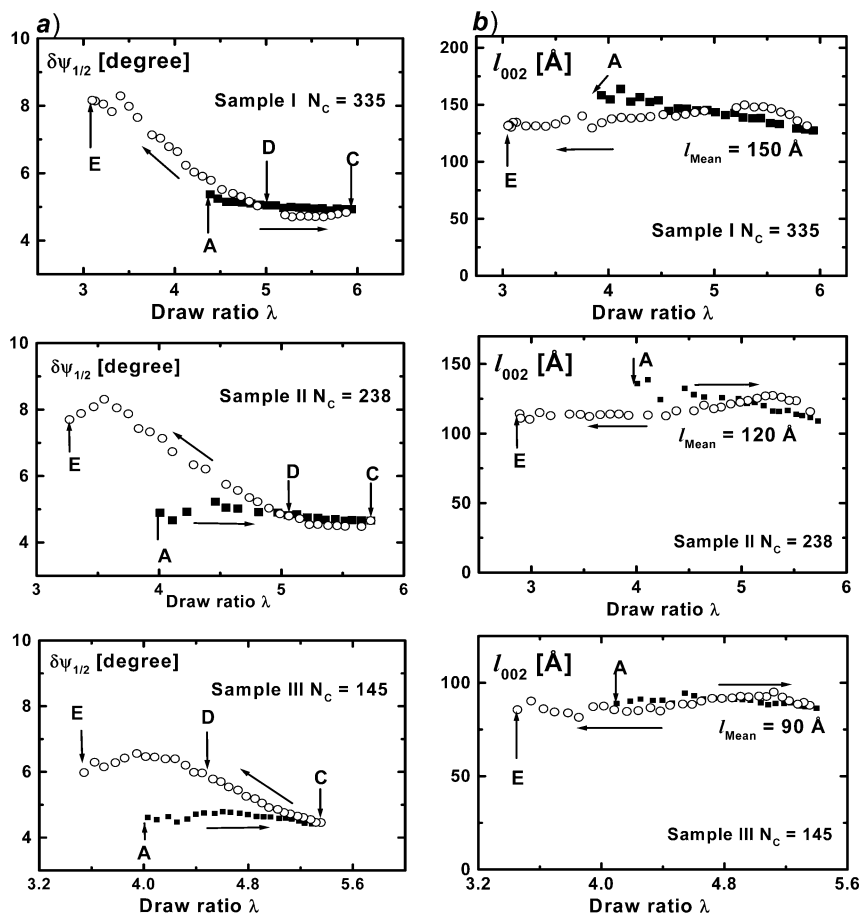
Figure 9. (a) Crystallites orientation $\delta\psi_{1/2}$ along the stretching direction. (b) Crystallites dimensions l_{200}, l_{120}, and l_{002} during cyclic deformation at $T = +23$ °C, strain rate $\dot{\epsilon} = 1$ mm/min, for the three different NR cross-linked samples ($N_C = 145$, 238, and 335)

as measured by the intensity of the (120) reflection, does not follow the quasi-linear law, $\chi(\lambda)$, observed here during recovery. It is emphasized that these authors did not take into account the variation of the absorption due to the change of thickness of their sample during deformation. These authors did not study the effect of the cross-link density on the curves $\chi(\lambda)$ and $\sigma(\lambda)$.

For all samples, during this recovery a weak disorientation of the crystallites occurs (Figure 9a shows that $\delta\psi_{1/2}$ increases from 4 to 8°), this is due to the relaxation of the stress. At the end of the melting process $\delta\psi_{1/2} = 8°$ corresponds to the observed value of sample in static deformation at $\lambda = 3$ (Figure 10b). Also it is noted that the crystallite size l_{002} remains constant (Figure 9b), whereas the crystallinity decrease linearly with λ. This effect is identical to what was observed during melting in static deformation (Figure 5). One concludes that during recovery at low strain rate the crystallites of constant dimensions melt gradually. In Figure 6c, the curves $T_m(\lambda)$ for the three samples **I**, **II**, **III** cross respectively the line $T_m = 23$ °C for $\lambda = 2.5$, 3, and 3.5. These values are exactly the values of λ_E deduced from the curves $\chi(\lambda)$ of Figure 8b. The temperature of experiment 23 °C, is the melting temperature $T_m(N_C)$ of the cross-linked material drawn at λ_E. One recalls that during recovery the local and macroscopic draw ratios are equal only when the traction and recovery curves $\sigma(\lambda)$ merge ($\lambda < \lambda_E$).

The different samples present very similar properties in static and continuous traction. In recovery, one observes a particular difference between the weakly

cross-linked sample and the others ones. At λ_D the crystallinity does not present any particular break in the $\chi(\lambda)$ curve for samples **II** and **III**, while for sample **I** a plateau of crystallinity is observed between λ_D and λ_E. This effect is described in the following section.

Remark: Inverse Yielding. For the less cross-linked sample **I** ($N_C = 335$), the recovery $\chi(\lambda)$ presents a plateau at λ_D, which is due to the appearance of a heterogeneous deformation in the material called "inverse yielding". This new effect is described in details in the Appendix. This sample ($N_C = 335$), along the DE portions of Figure 8, contains two deformed zones, semicrystalline and completely amorphous zones with volumes V_C and V_M, having respectively local constant draw ratio λ_D and λ_E. The existence of this plateau ($\chi_p(\lambda) = 15\%$) is due to the presence of this heterogeneity, as shown in the Appendix. One defines the average crystallinity $\langle\chi(\lambda)\rangle = \chi_C *(V_C/(V_C + V_M))$, where χ_C is the local crystallinity in the semicrystalline zone. This crystallinity verifies the relation (see Appendix):

$$\langle\chi\rangle = \chi_C \frac{1}{\lambda} \cdot \frac{\lambda - \lambda_E}{\lambda_D - \lambda_E} \qquad (14)$$

Here λ is the macroscopic draw ratio of the sample **I** ($N_C = 335$) $\lambda_D < \lambda < \lambda_E$.

In Figure 8b, this crystallinity $\langle\chi\rangle$ is represented by a heavy line between λ_D and λ_E for all samples. It is important to note that this relation fit also quantitatively the experimental crystallinity of the vulcanized rubbers (**II**, **III**), in which we do not observe the inverse
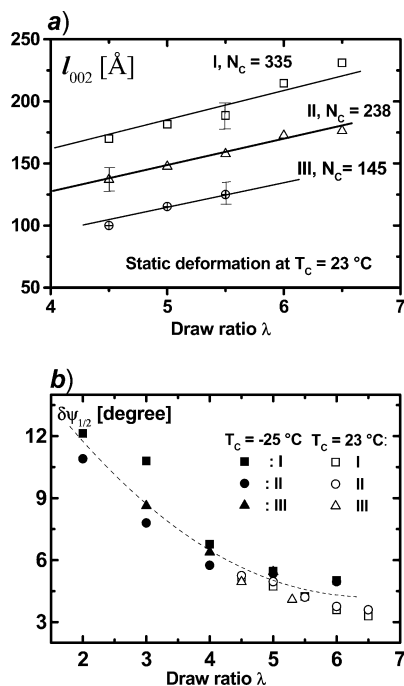
Figure 10. (a) Crystallites size l_{002} along the stretching direction and (b) orientation $\delta\psi_{1/2}$ as a function of draw ratio at $T_C = 23$ °C. The three different NR cross-linked samples ($N_c = 145$, 238, and 335) have been stretched at $T = 90$ °C and then quenched to $T_C = 23$ °C. $\delta\psi_{1/2}$ has been measured at ambient and -25 °C.

yielding phenomenon. This fact very probably indicates that a micro inverse yielding exists in all the samples (whatever is the cross-link density) but does not lead to any visible macroscopic instability for all. Why is this inverse yielding effect only observed in sample **I** ($N_C = 335$)? This is puzzling.

5. Origin of the Mechanical Hysteresis

The stress strain curves during traction and recovery do not coincide if the maximum draw ratio λ_{max} is greater than the critical draw ratio $\lambda_A = 4$ for the onset of crystallization. This effect confirms that the surface area between the two curves (mechanical hysteresis H) is due entirely to the phenomenon of crystallization and melting ($\lambda_A \neq \lambda_E$) and not to viscoelastic properties of the cross-linked rubber network. One recalls here that for any type of materials T_m is a thermodynamic parameter (there is no delay for melting) whereas T_C is not; the crystallization temperature T_C depends on the observation time, cooling rate, presence of nucleation agent, and the thermo mechanical history. In polymer materials the supercooling, $\Delta T = T_m - T_C$, is in general very high (20−60 °C), reaching 100 °C for polymers crystallizing near T_g. In stress-induced crystallization, it is difficult to analyze the hysteresis as a function of the supercooling ΔT because during the process this parameter ΔT is changing continuously. This effect is very similar to crystallization and melting of any material in concentrated solutions. During the first-order transition, the thermodynamic properties of the liquid amorphous phase change: for example the network chains in rubber become more relaxed and the concentration c of remaining crystallizable species in the solution decreases during isothermal crystallization. In both cases $T_m(\lambda)$ and $T_m(c)$ decrease with crystallization time. One analyzes hereafter the effect of cross-link density on the hysteresis in two particular cases.
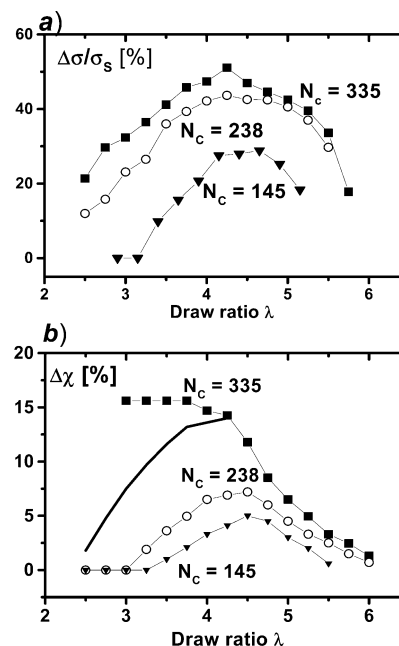

Figure 11. (a) Stress relaxation ratio $\Delta\sigma/\sigma_s = (\sigma_s - \sigma_r)/\sigma_s$ and (b) increase of crystallinity $\Delta\chi = \chi_r - \chi_s$ as a function of draw ratio during cyclic deformation at $T_C = 23$ °C, strain rate $\dot{\epsilon} = 1$ mm/min. $\Delta\sigma$ and $\Delta\chi$ of the NR cross-linked samples ($N_C = 145$, 238, 335) are indicated in Figure 8. The heavy line (recovery) for the sample **I** is obtained using relation 14. This sample presents an "inverse yielding instability"; see Appendix.

5.1. At Constant Maximum Draw Ratio. From Figure 8a, for each value of draw ratio, one has calculated the relative variation of the stress $\Delta\sigma/\sigma_s$, where $\Delta\sigma = \sigma_s - \sigma_r$ is the difference between the stresses during stretching σ_s and recovery σ_r at fixed λ. In Figure 11a, this relative stress difference is plotted vs draw ratio for the three vulcanized samples **I**, **II**, and **III**. $\Delta\sigma/\sigma_s$ present a flattened maximum. The width at half-height of the curve varies as the length of the plateau $\sigma(\lambda)$ of the recovery curve.

One calls $\Delta\chi = \chi_r - \chi_s$ the difference of crystallinities observed during traction χ_s and recovery χ_r (represented by curves [CE] and [CA] in Figure 8b). In Figure 11b, $\Delta\chi$ is plotted as a function of λ; here again one observes a difference between samples **I**, **II** and **III**. Sample **I** presents a plateau $\Delta\chi = 15\%$ for $\lambda < 4$, this is due to the inverse yielding effect. Using the average crystallinity $\langle\chi\rangle$ (relation 14) $\Delta\chi$ for sample **I** shows a decrease for $\lambda < 4$ (heavy line in Figure 8b). The crystallinity difference $\Delta\chi$ for the three samples presents a maximum between $\lambda = 4-4.5$.

For the three materials, one notes that $\Delta\chi$ and $\Delta\sigma/\sigma_s$ are correlated. The maximum observed for both parameters $\Delta\sigma/\sigma_s$ and $\Delta\chi$ are located around the middle of the plateau recovery, $(\lambda_E + \lambda_D)/2$. From Figure 11 one concludes that the mechanical hysteresis is due to the "crystallinity hysteresis", that is to say the crystallization and melting processes occur always at different temperatures (at λ fixed) or at different λ (at T fixed).

5.2. At Different Maximum Draw Ratios. Deformation cycles at the same strain rate $\dot{\epsilon} = 1$ mm/min and for different maximum draw ratio λ_{max} are given as an example in Figure 12a. During the same experiments the WAXS have been recorded. From mechanical and X-ray measurement one can make the following conclusions:
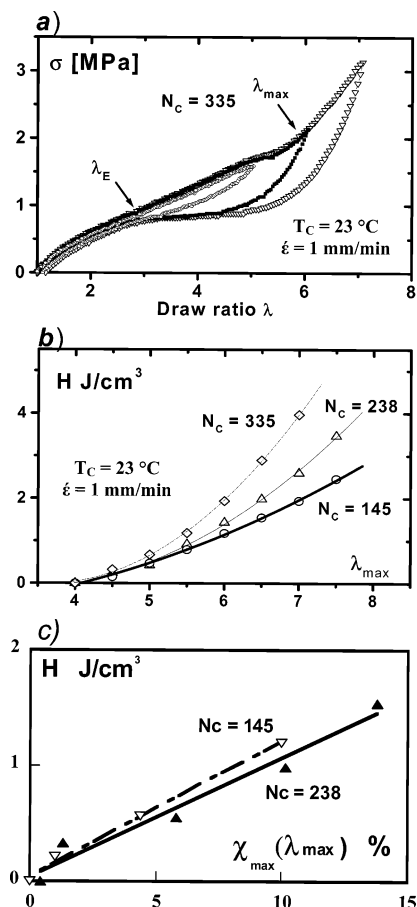
Figure 12. (a) Deformation cycles as a function of maximum draw ratio λ_{max}, sample **I** ($N_C = 335$) at $T_C = 23$ °C, strain rate $\dot{\epsilon} = 1$ mm/min. (b) Hysteresis H as a function of maximum draw ratio λ_{max} and cross-link density, same condition as in (a). (c) Hysteresis as a function of the crystallinity measured at the maximum draw ratio for samples **II** and **III**. Sample **I**, which presents a heterogeneous deformation, follows the same law when we plot H as a function of the mean crystallinity $\langle \chi \rangle$ defined in relation 14.

(a) The draw ratio λ_E is obviously independent of the maximum draw ratio λ_{max}.

(b) The hysteresis appears as soon as λ_{max} becomes higher than $\lambda_{max} = 4$.

(c) The plateau length of the recovery curve increases with λ_{max}.

All of these properties confirm that the mechanical hysteresis, which is on the order of $(\lambda_A - \lambda_E)\sigma_p/2$, is due only to the stress-induced crystallization (and stress-induced melting). More exactly, this hysteresis is due to the supercooling, that is to say to the difference between T_C (room temperature) and T_m (which depends on λ). During deformation cycles at the draw ratios λ_A and λ_E the crystallization $T_C(\lambda_A)$ and melting $T_m(\lambda_E)$ temperatures are equal to room temperature but the supercooling at these draw ratios are totally different. If the stress-induced crystallization would appear at equilibrium ($T_C = T_m$, $\lambda_A = \lambda_E$), then no hysteresis would be observed. It would be interesting to perform deformation cycles at very low strain rates to verify one the same material that H decreases with the difference $\lambda_A - \lambda_E$.

From the surface area between the stretching and recovery curves $\sigma(\lambda)$ one calculates the hysteresis H, corresponding to the mechanical energy lost per unit volume. H is plotted in Figure 12b as a function of λ_{max}

and N_C. One concludes that the hysteresis is an increasing function of the maximum draw ratio and a decreasing function of N_C. One verifies that H extrapolates to zero at the draw ratio $\lambda_{max} = \lambda_A$ (no crystallization) and that the less crystalline rubber (the highest cross-linked) presents the smallest hysteresis at fixed λ_{max}.

This relation between crystallinity and mechanical hysteresis can be seen in an other way. From Figure 8b, one knows the crystallinity (curve ABC) during stretching at 1 mm/min. During any cycle with maximum draw ratio $\lambda_{max} \leq 6$, the maximum crystallinity χ_{max} at λ_{max} is given by this curve, if the strain rate is the same. In Figure 12c, one has reported for samples **II** and **III** the hysteresis H as a function of the maximum crystallinity. In the domain $4 < \lambda < 6$, one concludes that H and χ_{max} verified the empirical law

$$H = 0.1\chi_{max} \text{ J/cm}^3, \quad R = 0.98 \qquad (15)$$

χ being in %. The same linear fit with similar correlation coefficients ($R = 0.95$) is observed for sample **I,** with the inverse yielding effect present. For $\lambda_{max} \leq 6$, one concludes that the relationship between hysteresis and maximum crystallinity is independent of the cross-link density. It would be interesting to verify if this relation holds above $\lambda_{max} = 6$. In this domain, rupture can occur ($\lambda_r = 8-9$), and the sample in the clamps begins to deform. These effects impede to draw any conclusion in the domain of high elongations.

6. Conclusions

We have studied in details the morphology of vulcanized natural rubber at nano scale, in static and in dynamic deformation. In vulcanized NR, the presence of cross-links impedes any effect of rearrangement and thickening of the crystallites in the early stage of crystallization. This has permitted to study the microscopic structure, the crystallites dimensions, and the crystallinity during isothermal and nonisothermal crystallization and during melting. The most important properties found in this work on drawn rubbers are the following.

In static deformation:

(a) The processes of crystallization (SIC) and melting (SIM) at constant deformation are similar, the crystallites sizes remain constant, and only the number of crystallites of constant volume changes during these first-order transitions. During these two processes, the crystallinity varies linearly with the retractive force (relation 9, and Figure 7), whatever the N_C value is.

(b) The crystallite sizes measured at −25 °C vary with the draw ratio λ according to the affine deformation laws (Figure 4). The crystallites volume V_C is independent of λ whatever is the cross-link density. V_C is about $1/4$ the volume per cross-link, which varies as $N_C^{1.5}$ (relation 3b).

(c) During isothermal crystallization the half time of crystallization log $t_{1/2}$ varies linearly with λ and N_C (Figure 2c). The dependency with λ is explained by the simple model of thermally activated motions (relation 7) and the fact that melting temperature T_m varies linearly with λ (relation 6). The effect of N_C is to shift by a same amount $\Delta\lambda$ the curves $T_m(\lambda)$ and log $t_{1/2}(\lambda)$.

In cyclic deformation at strain rate 1 mm/min:

(a) During stretching, crystallization appears at draw ratio $\lambda_A = 4$ independent of N_C, and during recovery, melting is gradual; the last crystals melt at a draw ratio

λ_E which increases with the density of cross-links. The value of λ_E is given by relation 6 and Figure 6c pertaining to vulcanized rubber at equilibrium. The λ_E values determined by WAXS and mechanical analysis coincide.

(b) During stretching and recovery the morphology obeys the same laws as in isothermal SIC and SIM. Crystallite sizes and c axis orientation remain constant (Figure 9; at low draw ratio during recovery a small disorientation is noted). The crystallinity increases linearly with the draw ratio. One concludes that the process of crystallization and melting are very similar in cyclic and static deformations.

(c) Stress hardening appears for a draw ratio $\lambda_B = 5$, somewhat higher than λ_A. The form of the stress strain traction curve $\sigma \sim \lambda^2$ above λ_B is explained by the fact that each new crystallite of constant volume V_C, which nucleate during stretching, is considered as a cross-link (relations 12 and 13).

(d) During the mechanical cycle for each value of λ the force $\Delta\sigma$ and crystallinity $\Delta\chi$ differences measured in traction and recovery are correlated (Figure 11). Mechanical hysteresis is due to the supercooling of the crystalline phase; the stress-induced crystallization (T_C) and melting (T_m) temperatures are different for a same draw ratio. In our experiments $T_C = T_m = 23$ °C but these two temperatures do not correspond to the same phase transition, the state (draw ratios λ_A, λ_E) of the amorphous phase being different.

(e) The mechanical hysteresis H depends on the maximum draw ratio λ_{max} and N_C values (Figure 12b), the maximum crystallinity χ_{max} obtained at λ_{max} is also dependent on these parameters. It is found that the mechanical hysteresis obeys the general law $H \sim \chi_{max}$ (relation 15, Figure 12c), independently of the values of N_C and λ. These properties concerning the relations between crystallinity and hysteresis reported in Figures 11 and 12 confirm that the viscoelastic properties of the amorphous chains must not be invoked for explaining the mechanical hysteresis.

The properties of cross-linked rubber reported in this work are surprising by their simplicity, they have not been predicted by the nucleation theories of crystallization. The Flory theory explains qualitatively some properties, as the relaxation of the force during crystallization and the amount of crystallinity. One has stated precisely in which temperature and strain domains this theory gives reasonable fits with the experimental data. These two types of theories, largely debated for half a century, fail in predicting the crystallite dimensions vs the distance between cross-links.

As noted earlier,[45,64] the distance between entanglements could be an important factor which limits the crystallinity and the crystallites size in semicrystalline polymers. It is also recognized that the entanglements slow the kinetics of crystallization. Depending on the time of experiment (or observation) in deformed polymers, entanglements can be considered as labile or nonlabile cross-links. In this work one has shown that the cross-links do limit the crystallinity and the kinetics of crystallization. Consequently we suggest that cross-links and entanglements play a same role in the process of crystallization: they limit crystallinity and crystallite sizes and impede local rearrangements of the chains and the agglomeration of small crystallites which would lead to the formation of large crystallite (and then lamellae) and well ordered spherulites (or shish-kebab structures).

One notes that the less cross-linked NR studied here has a molecular weight between cross-links $M_C = 64 N_C$ = 21440 Da; this is about the critical mass between entanglements[65] in poly(cis-isoprene) and polybutadiene melts, determined by viscoelasticity measurements. It would be interesting to study more deeply weakly vulcanized rubbers, when the density of cross-links is much smaller than the density of entanglements. We think that the properties reported here should be observed in non-vulcanized (crystallizable) polymers which do not flow during the time of experiment (high molecular weight polymer or/and branched polymers). In forthcoming papers, one will study the properties of carbon black filled rubbers and synthetic poly(cis-isoprene) rubbers.

Appendix

Figure 13a shows a series of images of this sample **I** ($N_C = 338$) taken during recovery ($\lambda_{max} = 6$). A heterogeneous deformation appears when the draw ratio reaches the value 4.8. It is generally, but not necessarily, initiated near the clamps. The sample becomes larger; the neck (arrows) separating two deformed zones propagates toward the middle of the material during recovery (at constant strain rate). In all materials, amorphous or semicrystalline, this type of heterogeneous deformation called yielding or necking occurs when the deformation increases. In polymers (like PP, PE, PET, and PS) this instability appears for a natural draw ratio about $\lambda_N = 2.4$. The exact value of λ_N depends on temperature and strain rate. We call this phenomenon appearing in sample **I** "inverse yielding" when the deformation decreases (recovery). By WAXS, it is controlled that the relaxed zone appearing near the clamps is not semicrystalline, and the other one which decreases in length during recovery has the same crystallinity as the starting material just before nucleation of the instability. If the macroscopic deformation is stopped, the system stays stable during time. The neck does not propagate; the two different zones (semicrystalline and non crystalline phases) are in equilibrium and have constant local draw ratio λ_D and λ_E. The length of the wider (amorphous) and thinner (semicrystalline) zones being $L_M(\lambda)$ and $L_C(\lambda)$, we have

$$\langle\chi\rangle = \chi_C \frac{L_M(\lambda)}{L_M(\lambda) + L_C(\lambda)} \qquad (16a)$$

The crystallinity χ_C is constant in the thinner zone. The relations between the two widths are

$$L_C + L_M = \lambda L_0; \quad L_C/\lambda_D + L_M/\lambda_E = L_0 \qquad (16b)$$

L_0 is the initial length of the sample. The second equation of relation 16b assumes that the sample volume is constant. Using these two relations, one finds relation 14.

Figure 13b gives the thickness t of the sample at the X-ray beam impact. It is obtained by measuring the attenuation of the X-ray beam and application of the Beer–Lambert law. During recovery from $\lambda = 6$ to $\lambda_D = 4.5$ (point D) the thickness follows the affine law, $t \approx 1/$
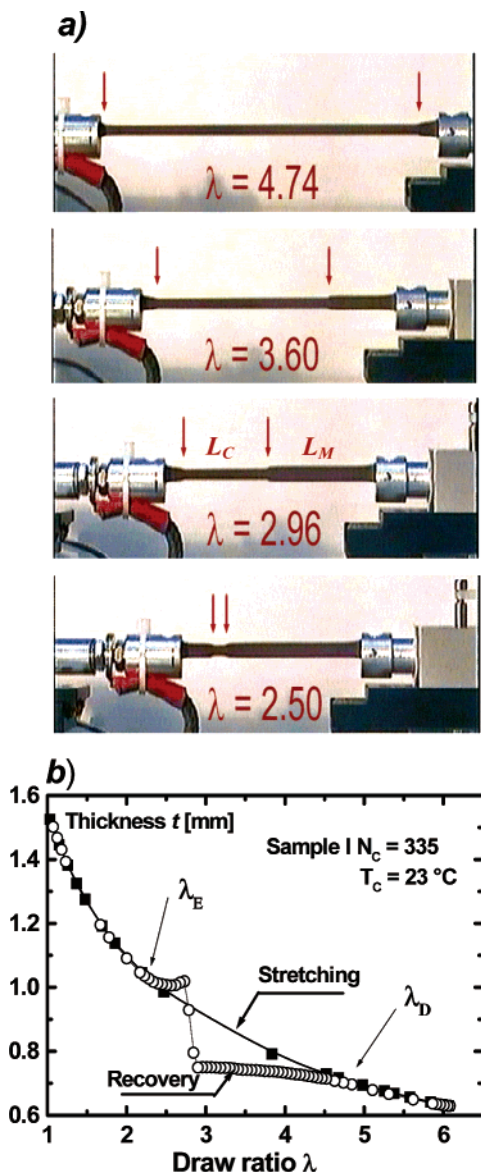
a)

λ = 4.74

λ = 3.60

L_C L_M

λ = 2.96

λ = 2.50

b)

Figure 13. (a) Series of images registered during recovery of sample **I** ($N_C = 335$) showing the phenomenon of "inverse yielding". The thin part of the sample between arrows is semicrystalline, the large ones near the clamps are completely amorphous. (b) Thickness t of sample **I** ($N_C = 335$) at the X-ray beam impact during the mechanical cycle, strain rate $\dot\epsilon = 1$ mm/min. the thickness jump observed at $\lambda = 2.8$ is due to the passage of the yield neck through the X-ray beam.

$\sqrt{\lambda}$. Below λ_D (Figure 13b), the thickness remains constant (at the X-ray impact), when the yield neck passes through the X-ray beam. At the critical draw ratio $\lambda_E = 2.5$, the crystallinity has disappeared and the yield has totally swept all the length of the sample. At this time, the thickness t suddenly increases and follows again the affine law.

References and Notes

(1) Smith, J. R.; Greene. K.; Ciferri, J. A. *Kolloid-Z. Z. Polym.* **1962**, *49*, 194.
(2) Alexander, L. E.; Ohlberg, S.; Taylor, G. R. *J. Appl. Phys.* **1955**, *26*, 1068.
(3) (a) Luch, D.; Yeh, G. S. Y. *J. Macromol. Sci. Phys.* **1973**, *B7*, 121. (b) Hardin, I. R.; Yeh, G. S. Y. *J. Macromol. Sci. Phys.* **1973**, *B7*, 393.
(4) Mitchell, G. R. *Polymer* **1984**, *25*, 1562.
(5) Siesler, H. W. *Appl. Spectrosc.* **1985**, *39*, 761.
(6) Choi, I. S.; Roland, C. M. *Rubber Chem. Technol.* **1997**, *70*, 202.
(7) Siesler, H. W. *Appl. Spectrosc.* **1985**, *39*, 761.
(8) Shimomura, Y.; White, J. L.; Spruiell, J. E. *J. Appl. Polym. Sci.* **1982**, *27*, 3553.
(9) Mukherjee, D. P. *Rubber Chem. Technol.* **1974**, *47*, 1234.
(10) Taylor, G. R.; Darin, S. R. *J. Appl. Phys.* **1955**, *26*, 1075.
(11) Andrews, E. H. *Proc. R. Soc. London, Ser. A* **1964**, *A277*, 562.
(12) Andrews, E. H. *J. Polym. Sci.* **1966**, *A-2*, 4, 668.
(13) Andrews, E. H. *Pure Appl. Chem.* **1972**, *31*, 91.
(14) Andrews, E. H.; Owen, P. J.; Singh, A. *Rubber Chem. Technol.* **1972**, *45*, 1315.
(15) (a) Luch, D.; Yeh, G. S. Y. *J. Appl. Phys.* **1972**, *43*, 4326. (b) Hardin, I. R.; Yeh, G. S. Y. *J. Macromol. Sci. Phys.* **1973**, *B7*, 375.
(16) Tsuji, M.; Shimizu, T.; Kokjiya, S. J. *Polymer.* **2000**, *32*, 505.
(17) Shimizu, T.; Tosaka, M.; Tsuji, M.; Kokjiya, S. *Rubber Chem. Technol.* **2000**, *73*, 926.
(18) (a) Gent, A. N. *Trans. Faraday Soc.* **1954**, *50*, 521. (b) Gent, A. N. *J. Polym. Sci., Part A:* **1965**, *3*, 3787. (c) Gent, A. N. *J. Polym. Sci., Part A:2* **1966**, *V4*, 447.
(19) Goritz, D.; Muller, F. H.; Sietz, W. *Prog. Colloid Polym. Sci.* **1977**, *62*, 114.
(20) Kim, H. G.; Mandelkern, L. *J. Polym. Sci. A-2* **1968**, *6*, 181.
(21) Sietz, W.; Goritz, D.; Muller, F. H. *Prog. Colloid Polym. Sci.* **1978**, *64*, 267.
(22) Gent, A. N.; Kawahara, S.; Zhao, J. *Rubber Chem. Technol.* **1997**, *71*, 668.
(23) Gent, A. N.; Zhang, L. Q. *J. Polym. Sci., Polym. Phys.* **2001**, *39*, 811.
(24) Luch. D.; Yeh. G. S. Y. *J. Polym. Sci.* **1973**, *11*, 467.
(25) Mitchel, J. C.; Meier, D. J. *J. Polym. Sci., Part A2.* **1968**, *6*, 1689.
(26) Gent, A. N. *Engineering with Rubber*; Hanser Publishers, Oxford University Press: Oxford, England, 1992.
(27) Payne, R. *J. Polym. Sci.* **1974**, *48*, 169.
(28) Doherty, W. O. S.; Kim, L.; Treloar, L. R. G. *J. Br. Polym.* **1980**, 19.
(29) Hamed, G. R. Ref 23, Chapter 3, p 11. Hamed, G. R. *Rubber Chem. Technol.* **1990**, *64*, 493.
(30) Gent, A. N. *Rubber Chem. Technol.* **1996**, *69*, 59.
(31) Treloar, L. R. G. *The Physics of Rubber Elasticity*, Oxford University Press: London, 1975.
(32) Boyce. M. C. *Rubber Chem. Technol.* **1996**, *69*, 581.
(33) Boyce, M. C.; Arruda. E. M. *Rubber Chem. Technol.* **2000**, *73*, 504.
(34) Flory. P. J. *J. Chem. Phys.* **1947**, *15*, 397.
(35) Krigbaum. W. R.; Roe R. J. *J. Polym. Sci.* **1964**, *A2*, 4391.
(36) Gaylord, R. J. *Polym. Lett. Edit.* **1975**, *13*, 337; *J. Polym. Sci. (Polym. Phys. Edit.)* **1976**, *14*, 1827.
(37) Gaylord, R. J.; Lohse, D. *J. Polym. Eng. Sci.* **1976**, *16*, 163.
(38) Smith, K. *J. Polym. Eng. Sci.* **1976**, *16*, 168.
(39) Elyashevich, G. K.; Baranov, V. G.; Frenkel. S. Y. *J. Macromol. Sci. Phys.* **1977**, *B13*, 255.
(40) Negahban, M. *Int. J. Solids Struct.* **2000**, *37*, 2777.
(41) Mandelkern, L. *Crystallization of polymers*; McGraw-Hill: New York, 1964.
(42) Geil, P. H. *Polymer Single Crystals; Interscience*: New York, 1963.
(43) Strobl, G. *Physics of Polymers*; Springer, Berlin, 2001.
(44) Rault, J.; Souffache, E. *J. Polym. Sci., Phys.* **1989**, *27*, 1349.
(45) Souffache, E.; Rault. J. *Macromolecules* **1989**, *22*, 3581.
(46) Rault, J. *J. Macromol. Sci., Chem. Phys. Rev.* **1997**, *C37*, 335.
(47) Toki, S.; Fujimaki, T.; Okuyama, M. *Polymer* **2000**, *41*, 5423.
(48) Toki, S.; Sics, I.; Ran, S.; Liu, L.; Hsiao, B. S.; Murakami, S.; Senoo, K.; Kohjiya, S. *Macromolecules* **2002**, *35*, 6573.
(49) Murakami, S.; Senoo, K.; Toki, S.; Kohjiya, S. *Polymer* **2002**, *43*, 2117.
(50) Klug, H. P.; Alexander, L. E. *X-ray Diffraction Procedures*; Wiley: New York, 1954.
(51) *International Tables for Crystallography*; Kluwers Academic Publ.: Dordrecht, The Netherlands, 1995; Vol. C, p 520.
(52) Benedetti, E.; Corradini, P.; Pedone, C. *Eur. Polym.* **1975**, *11*, 585.
(53) Alexander, L. E. *X-ray Diffraction Methods in Polymer Science*; Wiley: New York, 1969.
(54) Dumbleton, B.; Bowles, B. *J. Polym. Sci., Part A2* **1966**, *4*, 951.
(55) Lee, D. J.; Donovan, J. A. *Rubber Chem. Technol.* **1987**, *60*, 910.
(56) Trabelsi, S.; Albouy, P. A.; Rault, J. *Macromolecules* **2002**, *35*, 10054.

(57) Langford, J. L.; Wilson, A. J. C. *J. Appl. Crystallogr.* **1978**, *11*, 102.
(58) Lovel, R.; Mitchell, G. R. *Acta Crystallogr.* **1980**, *A37*, 135.
(59) Rahman, N.; Isanasari, A.; Anggraeni, R.; Honggokusumo, S.; Iguchi, M.; Masoku, T.; Tashiro, K. *Polymer* **2003**, *44*, 283.
(60) Rault, J. *J. Macromol. Sci.* **1978**, *B13*, 4.
(61) *Polymer Handbook*; Mark, J. E., Ed.; IntersciencePublishers: New York, 1963.

(62) Rault, J. To appear in *J. Macromol. Sci. Phys.* **2003**.
(63) Dalal, E. N.; Taylor, K. D.; Phililips, P. J. *Polymer* **1983**, *24*, 1623.
(64) Rault, J. *Faraday Discuss. Chem. Soc.* **1979**, *68*, 367 and 370.
(65) Ferry, D. *Viscoelastic Properties of Polymers*; Wiley: New York, 1967.